Non-oxidative coupling of methane over Pd-loaded gallium oxide photocatalysts in a flow reactor

Surya Pratap Singh,[a] Akihiko Anzai,[a] Satoru Kawaharasaki,[a] Akira Yamamoto,[a,b] and Hisao Yoshida[a,b,*]

Affiliation and full postal address

[a] *Department of Interdisciplinary Environment, Graduate School of Human and Environmental Studies, Kyoto University, Yoshida Nihonmatsu-cho, Sakyo-ku, Kyoto 606-8501, Japan*

[b] *Elements Strategy Initiative for Catalysts & Batteries (ESICB), Kyoto University, Kyotodaigaku Katsura, Nishikyo-ku, Kyoto 615-8520, Japan*

Corresponding author

Professor Hisao Yoshida

Department of Interdisciplinary Environment,

Graduate School of Human and Environmental Studies,

Kyoto University,

Yoshida Nihonmatsu-cho, Sakyo-ku, Kyoto 606-8501, Japan.

Tel: +81–75–753–6594 Fax: +81–75–753–2988

E–mail address: yoshida.hisao.2a@kyoto-u.ac.jp

Abstract

Photocatalytic methane conversion is attractive for utilization of renewable biogas and solar energy to directly produce useful compounds. In the present study, gallium oxide (Ga_2O_3) photocatalyst was examined for non-oxidative coupling of methane (NOCM) around room temperature in a flow reactor. It was found that ethane and hydrogen were continuously yielded at constant rate from methane upon photoirradiation around room temperature, confirming that NOCM can be promoted photocatalytically over Ga_2O_3. In addition, Pd cocatalyst was found to improve the activity of the Ga_2O_3 photocatalyst for NOCM and achieve more than three times higher formation rate of ethane such as 0.22 μmol h^{-1} in a flow of 10% methane at 30 mL min^{-1} with 0.8 g of photocatalyst. The methane conversion achieved to 0.006% within a short contact time of 0.8 s, which is higher than the thermodynamically equilibrium conversion.

Keywords: Methane conversion; Ethane production; C-C coupling; Gallium oxide; Palladium; Photocatalysis.

1. Introduction

Methane, the main component of natural gas as well as biogas, has attracted much attention as one of alternative resources for carbon and hydrogen to replace finite resources like petroleum. Among many kinds of catalytic reaction systems, such as reforming, partial oxidation, and oxidative coupling [1–5], non-oxidative coupling of methane (NOCM) is one of desirable reactions to directly produce ethane and hydrogen from methane (eq. 1) [6–8].

$$2\ CH_4 \rightarrow C_2H_6 + H_2, \qquad \Delta_r G^{\Theta}_{298K}=68.6\ \text{kJ mol}^{-1} \quad (1)$$

This is, however, a thermodynamically unfavorable endergonic reaction and the equilibrium constant and equilibrium conversion of this reaction at 298 K are very low such as 9.5×10^{-13} and 0.0002 %, respectively, meaning that this reaction does not take place at 298 K in practice [9]. Although the equilibrium conversion becomes higher at higher temperatures, such as 1.1% and 7.2% at 800 K and 1273 K, respectively, decomposition of methane to carbon and hydrogen (eq. 2) is not negligible at temperatures higher than 800 K because it is thermodynamically more favorable than NOCM [9].

$$CH_4 \rightarrow C + 2H_2, \qquad \Delta_r G^{\Theta}_{298K}=50.7\ \text{kJ mol}^{-1} \quad (2)$$

Over the last few decades, photocatalyst has become attractive, since it can utilize solar energy to compensate the increase of the chemical potential and to promote thermodynamically unfavorable reactions even at room temperature. In other words, by photocatalysis solar energy can be converted and stored as chemical potential of the products. Photocatalytic NOCM has also been reported since 1998 with various photocatalysts such as SiO_2-Al_2O_3 [10–12], SiO_2-Al_2O_3-TiO_2 [13,14], Ga/SiO_2 [15], and so on [9,15–24]. Most of them are silica-based quantum photocatalysts having atomically

dispersed photocatalytic active sites in silica matrix [25,26], where one of important properties for these photocatalysts would be a reduction-resistant property in the highly reductive conditions, i.e., in the presence of methane, ethane and hydrogen upon photoirradiation. Recently, some silica-based photocatalysts [27,28] and other types of photocatalysts such as plasmonic photocatalyst [29] have been reported for NOCM. However, it is noted that all these studies have examined the photocatalysis in a closed reactor so far, which is not sufficient for exact evaluation of catalytic reaction rate.

In our latest study, gallium oxide (Ga_2O_3) was found to function as a photocatalyst for NOCM [15,30]. Photocatalytic property of Ga_2O_3 has been studied so far for various reactions such as water splitting [31–33], photodegradation of organic compounds [34,35], reforming of methane with carbon dioxide [30,36] or water [37–39], and reduction of carbon dioxide with hydrogen [40] or water [41–46]. In the present study, we examined Ga_2O_3 photocatalyst for NOCM in a flow reactor to elucidate whether the photocatalytic NOCM reaction can be continuously promoted or not, and to evaluate the exact production rates of ethane and hydrogen with the Ga_2O_3 photocatalyst. In addition, we tried to improve the activity of the Ga_2O_3 photocatalyst by loading some additives and found that a Pd cocatalyst improved the activity of the Ga_2O_3 photocatalyst for NOCM.

2. Experimental

2.1 Catalyst preparation

The employed Ga_2O_3 sample was commercially obtained (Ga_2O_3, 99.90%, Kojundo Chemical Laboratory). The following chemicals were used as precursors of additives, $Pt(NH_3)_4(NO_3)_2$ (99.0%, Nacalai Tesque), $RhCl_3$ (98%, Wako Pure Chemical), $PdCl_2$ (99%, Kishida Chemical), $AgNO_3$ (99.8%, Kishida Chemical), $Ni(NO_3)_2 \cdot 6H_2O$

(99.9%, Wako Pure Chemical), $Fe(NO_3)_3 \cdot 9H_2O$ (99%, Nacalai Tesque), $In(NO_3)_3 \cdot 3H_2O$ (98% Kishida Chemical), $Zn(NO_3)_2 \cdot 6H_2O$ (99%, Nacalai Tesque), and $Sm(NO_3)_3 \cdot 6H_2O$ (99.5%, Wako Pure Chemical). Each additive metal or metal oxide was loaded on the Ga_2O_3 sample by an impregnation method: The Ga_2O_3 powder sample (2.0 g) was stirred in an aqueous solution of the precursor (100 mL) at room temperature for 30 min, followed by heating at 353 K to evaporate water to dryness. The obtained powder was dried at 373 K overnight and calcined in an alumina crucible by using an electric muffle furnace at 673 K for 2 h. The metal- or metal oxide-loaded samples are referred to as M(*x*)/Ga_2O_3 sample, where *x* in wt% shows loading amount of the additive (M) calculated as a metal state even if it was oxidized, for example, Pd(0.5)/Ga_2O_3.

2.2 Characterization

The obtained samples were characterized by several techniques. The crystal structure was determined by powder X-ray diffraction with a Shimadzu LabX XRD-6000 X-ray diffractometer using Cu K_α radiation (40 kV, 30 mA). Scanning electron microscope (SEM) images were recorded on a JEOL model JSM-890 scanning microscope. Diffuse reflectance UV-visible spectra were recorded by a JASCO V-570 UV/VIS/NIR spectrophotometer equipped with an integrating sphere covered with a $BaSO_4$ reference. The BET specific surface area of the Ga_2O_3 sample was measured by a Quantachrome Monosorb rapid surface area analyzer. The loading amount of Pd was estimated by X-ray fluorescence (XRF) technique using a Shimadzu EDX-8000 energy dispersive X-ray fluorescence spectrometer.

2.3 Photocatalytic activity tests

The photocatalytic activity test for non-oxidative coupling of methane (NOCM) was carried out using a flow reactor shown in Fig. S1 (supplementary information) [47–50]. The catalyst powder was pressed under 40 MPa and ground into granules of 297–707 μm (25–50 mesh). The sample granules (0.8 g) were placed into a quartz cell (2 × 2 × 0.1 cm^3, see the picture shown in Fig. S2). The sample was pretreated with an argon flow for 30 min (flow rate = 27 mL min^{-1}) to remove the air from the quartz cell. A flow of mixture of 10% methane in argon (total flow rate = 30 mL min^{-1}) was introduced to the cell for 1 h in dark to achieve stable conditions, where the contact time was nearly 0.8 s and space velocity (SV) was 4500 h^{-1}. The sample was then photoirradiated from a ceramic xenon lamp (PE300BUV, 300 W) to start the photocatalytic NOCM. The irradiation area was 4 cm^2 and the light intensity as a standard was *ca.* 20 mW cm^{-2}, which was measured at 254±10 nm in wavelength. The reaction temperature was increased to be around 320 K by photoirradiation. The outlet gases were analyzed by on-line gas chromatography equipped with TCD (Shimadzu, GC-8A, argon carrier, a Molecular Sieves 5A, column temperature 323 K) and FID (Shimadzu, GC-8A, argon carrier, a Gaskuropack 54, column temperature 383 K). Methane conversion is calculated based on the amount of obtained products as described in the supplementary information (eq. S1).

3. Results and discussion

3.1. Gallium oxide photocatalyst

The bare Ga_2O_3 powder sample was characterized by some techniques. The XRD pattern of the bare Ga_2O_3 sample (Fig. 1b) was almost similar to that of β-Ga_2O_3 crystal

from a database (Fig. 1a, ICSD#34243 [51]) except for some additional diffraction lines at 24.5, 33.8, 36.2, 41.5, 50.3 and 55.1 degrees assigned to α-Ga_2O_3 phase (ICSD#27431 [52]). Among them the line at 36.2 degrees is somewhat large, which is assignable also to γ-Ga_2O_3 phase (ICSD#152085 [53]). This result means that the commercially obtained Ga_2O_3 sample is of mixed crystal mainly consisting of β-Ga_2O_3 phase including minor amount of α-Ga_2O_3 and γ-Ga_2O_3 phases. The SEM image of the bare Ga_2O_3 sample is shown in Fig. 2A. Pillar-shaped layered particles with some cracks having an average length of 1 μm were observed for the bare Ga_2O_3 sample as reported in the literature [54]. Fig. 3 shows diffuse reflectance UV-visible spectra of the samples. The bare Ga_2O_3 sample exhibited a large absorption in the range of shorter wavelength less than 270 nm (Fig. 3a), from which the bandgap was calculated to be around 4.6 eV. The measured BET specific surface area of the bare Ga_2O_3 sample was 22.8 m^2 g^{-1}.

Fig. 4 shows time courses of the production rates of ethane (r_C) and hydrogen (r_H) and the ratio of these reaction rates ($R=r_C/r_H$) obtained in the photocatalytic reaction test for NOCM in a flow reactor at around room temperature (*ca.* 320 K) over the bare Ga_2O_3 sample. No product was observed in dark, while upon photoirradiation both ethane and hydrogen were continuously produced with almost constant formation rates at least for 5.5 h and no other product in gas phase was detected. The formation rate for ethane and hydrogen were 0.073 and 0.18 μmol h^{-1}, respectively after 5.5 h under photoirradiation and the ratio of these reaction rates was R=0.41 (Table 1, entry 1). The relatively higher rate of hydrogen production than that of ethane would be attributed to the other reaction, which should be a side reaction such as methane decomposition (eq. 2) as discussed later. The methane conversion was calculated to be around 0.002% in constant, which was much higher than the equilibrium conversion [9].

3.2. Metal-loaded gallium oxide photocatalysts

In order to improve the photocatalytic performance of the Ga_2O_3 sample, several metal and metal oxide species were examined as a cocatalyst. Each species was loaded on the Ga_2O_3 photocatalyst by an impregnation method followed by calcination. Representatively, the prepared Pd(x)/Ga_2O_3 samples were characterized by XRD, SEM and UV-Vis spectra. XRD patterns of all the Pd(x)/Ga_2O_3 (x=0.05, 0.1, and 0.5 wt%) samples were almost the same as those of the bare Ga_2O_3 sample (Fig. 1c–1e). Besides no additional peak appeared in the XRD patterns of these Pd(x)/Ga_2O_3 samples, meaning that Pd species is highly dispersed in the crystal lattice of Ga_2O_3 and does not form any new crystal phase. The SEM image of the Pd(0.5)/Ga_2O_3 sample is shown in Fig. 2B. Although the fragments of the Ga_2O_3 particles seem to increase during the impregnation and stirred in an aqueous solution, no Pd species were clearly confirmed due to the small loading amount such as 0.5 wt%. Loading of the Pd nanoparticles has no significant effect on the morphology and the particle size of the bare Ga_2O_3 sample. The shape of diffuse reflectance UV-Vis spectra of the Pd(x)/Ga_2O_3 samples (Fig. 3b-3d) at shorter wavelength range were almost similar to the bare Ga_2O_3 sample while absorption in the range of 280–500 nm in wavelength increased with increasing Pd loading amount in the Pd(x)/Ga_2O_3 samples probably due to the Pd species [55]. This suggests that the impregnation method followed by the calcination at 673 K provides the metal or metal oxide species on the Ga_2O_3 surface without changing the band structure of Ga_2O_3 drastically [37]. The elemental composition of Pd in various Pd(x)/Ga_2O_3 (x=0.01–1.0 wt%) samples was analyzed by XRF and the results are listed in Table S1, which confirmed the aimed amount of Pd cocatalyst was almost loaded on each Pd/Ga_2O_3 sample.

Fig. 5 shows time courses of the production rates over the Pt- and Pd-loaded Ga_2O_3 samples. The Pt(0.1)/Ga_2O_3 sample initially exhibited formation of ethane and hydrogen at the rates of 0.04 and 3.01 μmol h^{-1}, respectively (Fig. 5A), which were lower and very higher than those with the bare Ga_2O_3 sample, 0.078 and 0.21 μmol h^{-1}, respectively (Fig. 4). The formation rates then steeply decreased with time and reached 0.023 and 1.6 μmol h^{-1}, respectively after 5.5 h under photoirradiation (also Table 1, entry 2). The production ratio of ethane to hydrogen was very low such as R=0.01. After this reaction test, the color of the Pt(0.1)/Ga_2O_3 sample varied from white to grey (Fig. S2). The high hydrogen formation rate and the color change suggested that methane decomposition to carbon and hydrogen (eq. 2) would take place to form coke on the surface of the Pt(0.1)/Ga_2O_3 sample even at 320 K, which would be catalyzed by the additive Pt species.

On the contrary, the Pd(0.5)/Ga_2O_3 photocatalyst exhibited constant formation of ethane and hydrogen after an induction period of a few hours (Fig. 5B). The formation rates of ethane and hydrogen after 5.5 h were 0.22 and 0.23 μmol h^{-1}, respectively (Table 1, entry 6). The ethane formation rate over this sample was more than three times higher than that with the bare Ga_2O_3 sample, 0.073 μmol h^{-1} (Table 1, entry 1). The production ratio of ethane to hydrogen was almost unity, R=1.0, meaning that photocatalytic NOCM proceeded constantly with high selectivity according to equation 1. The methane conversion was calculated to be 0.008–0.006% during 5.5 h. After the reaction test, the color of the sample did not change so much, supporting that the NOCM selectively took place while methane decomposition would scarcely occur.

Results over the M(x)/Ga_2O_3 samples loaded with other additives are also listed in Table 1. Among the examined elements, only Pd and Ag additives enhanced the ethane formation rate with moderate hydrogen production (Table 1, entries 4–7 and Fig. S3).

Effect of loading amount of Pd cocatalysts upon the photocatalytic activity is summarized in Table S1. Among various Pd(x)/Ga_2O_3 samples with different loading amounts, the Pd(0.1)/Ga_2O_3 sample showed the highest ethane formation rate of 0.51 μmol h^{-1} (Table 1, entry 5), while the Pd(0.5)/ Ga_2O_3 sample exhibited similar formation rates for both ethane and hydrogen with the highest R value close to unity as mentioned above (Table 1, entry 6). It is notable that in many cases including the bare Ga_2O_3 photocatalyst, the R value was lower than unity, meaning that methane decomposition (eq. 2) tends to take place even at 320 K in the present photocatalytic reaction conditions. Especially, Pt and Rh species exhibited very high production rate of hydrogen and low production rate or no formation of ethane, meaning that these precious metals much enhanced methane decomposition (Table 1, entries 2, 3). Thus, it is suggested that Pd and Ag species can enhance not the methane decomposition but the photocatalytic NOCM.

In the present study, the Pd-loaded Ga_2O_3 photocatalysts were the best photocatalysts for NOCM. Since the formation rate per photocatalyst weight were often reported in literature [27–29], the values for the Pd(0.5)/Ga_2O_3 photocatalyst were tentatively calculated to be 0.28 and 0.29 μmol h^{-1} g^{-1} for ethane and hydrogen formation, respectively. However, it is noted that this evaluation would not be accurate because the reaction rate was not linear to the catalyst weight but rather determined by the irradiation area in this type of flow reactor [56]. Further investigation is required on this point.

3.3. Reaction conditions

Without photoirradiation, NOCM did not proceed over the Pd(0.5)/Ga_2O_3 sample at similar temperature, 323 K, and even at elevated temperatures such as 573 K and 623 K. (Table 1, entries 13–15). Thus, it is evident that NOCM can proceed only under

photoirradiation even at high temperature. At high temperature such as 623 K, the formation of hydrogen only was observed (Table 1, entry 15), meaning that decomposition of CH_4 to C and H_2 would occur in dark, which is supported by the dark grey color of the sample after the reaction (Fig. S4). This implies that thermal energy given at higher temperature can promote not NOCM but methane decomposition.

The photocatalytic NOCM was examined at higher intensities of incident light than 20 $mWcm^{-2}$, over the Pd(0.05)/Ga_2O_3 photocatalyst for 5 h (Fig. 6). When comparing the results with the intensity of 20 and 40 $mWcm^{-2}$, the production rate of ethane was higher for the higher light intensity such as from 0.35 to 0.42 $\mu mol\ h^{-1}$ as expected. But further increase of the light intensity decreased the ethane production rates. Very high light intensities, such as 145 and 230 $mWcm^{-2}$, caused methane decomposition predominantly, which was supported by the color change (Fig. S5). The selectivity of ethane is much decreased with an increase in intensity of light higher than 75 mW cm^{-2}. These observations elucidate that the moderate light intensity is favorable for the selective photocatalytic NOCM over the Pd-loaded Ga_2O_3 photocatalyst.

It is generally accepted that photocatalysis with semiconductor photocatalyst starts from light absorption by the photocatalyst, electrons are photoexcited from the valence band to the conduction band with generating positive holes in the valence band simultaneously, and the generated electrons and holes can react with molecules and ions adsorbed on the surface of the photocatalyst. In the photocatalytic NOCM, the following mechanism has been typically proposed to proceed predominantly [29]. Since methane cannot be further reduced, the first activation of methane must be oxidation by the photogenerated positive hole to form methyl radical and proton on the photocatalyst surface (eq. 3) and two methyl radicals would react to form ethane (eq. 4), while two protons formed should be reduced

by the photogenerated electrons to form hydrogen molecule (eq. 5).

$CH_4 + h^+ \rightarrow \bullet CH_3 + H^+$ (3)

$2 \bullet CH_3 \rightarrow C_2H_6$ (4)

$2 H^+ + 2 e^- \rightarrow H_2$ (5)

The higher light intensity accelerates the hole oxidation rate, which would promote not only the methyl radical formation (eq. 3) but also further oxidation successively on the surface (eq. 6) before desorption of these produced radical species, along with the hydrogen formation (eq. 5), which is a proposed mechanism for methane decomposition on the surface (eq. 2).

$\bullet CH_3 + 3 h^+ \rightarrow C + 3 H^+$ (6)

As shown in Fig. S6, the reaction with high light intensity (145 $mWcm^{-2}$) caused a decrease of the ratio of the production rates, *R*, with time. This suggests that, even if the high light intensity increased the reaction rates of both the NOCM (eq. 1) and the methane decomposition (eq. 2), the latter reaction makes coke deposition on the surface and the accumulation of coke deposition on the surface with time would change the surface property to decrease the activity for the photocatalytic NOCM or enhance the methane decomposition. It may also be possible that photoenergy and thermal energy synergistically accelerate the coke formation at higher light intensities since the temperature at 230 $mWcm^{-2}$ was measured to be around 160°C.

Effect of methane concentration in the feed gas was examined on the photocatalytic NOCM over the Pd(0.05)/Ga_2O_3 photocatalyst (Fig. 7). When the methane concentration was increased from 10 % and 80%, the ethane production rate increased from 0.35 to 0.51 $\mu mol\ h^{-1}$, which is kinetically expected. On the other hand, the ratio of the production rates, *R*, decreased with increasing methane concentration at higher methane

concentrations such as 80% and 100%. This means that the rate of methane decomposition become higher in these conditions. The higher concentration of methane should increase the photocatalytic reaction rates of both the NOCM and the methane decomposition, and the latter reaction would give the coke deposition to change the reaction selectivity as discussed above.

Finally, the effect of the flow rates of the feed gas was investigated on the photocatalytic NOCM over the Pd(0.05)/Ga_2O_3 photocatalyst. As demonstrated in Fig. 8, with increasing the flow rate, the ethane formation rate increased while the hydrogen formation rate decreased. Thus, the ratio of the reaction rates, *R*, increased with the flow rate towards the unity, meaning that the NOCM selectivity increased with the flow rate. This suggests that the higher flow rate may help the migration of radical species to enhance the coupling (eq. 4, 5) before further hole oxidation (eq. 6–8), making the NOCM selectivity high. At the slow flow rate such as 10 mL min^{-1}, tiny amount of propane formation was also observed. This proposes that the longer contact time would provide the possibility for the successive coupling reactions to produce higher hydrocarbons such as propane and so on.

4. CONCLUSIONS

In conclusion, by using a flow reactor it was evidenced that the photocatalytic non-oxidative coupling of methane (photocatalytic NOCM) can be promoted over the Pd(0.5 wt%)/Ga_2O_3 photocatalyst almost constantly at least for 5.5 h with the ideal production ratio of ethane and hydrogen, R=1.0, i.e., with high selectivity. The ethane production rate was high such as 0.22 μmol h^{-1}, and methane conversion was 0.006% in the present conditions where the contact time (reaction time) and space velocity (SV) were 0.8 s and

4500 h^{-1}, respectively. The conversion clearly exceeded the thermodynamic equilibrium conversion at this temperature.

It was also found that the moderate light intensity, the moderate methane concentration, and the higher flow rates of the feed gas are favorable for the NOCM reaction over Pd/Ga_2O_3 photocatalysts. Instead, methane decomposition to form coke deposition can proceed as a side reaction under the following conditions, at higher temperature such as 320 K even in dark, at high light intensity, in the high methane concentration, and in a slow flow rate, which is a remaining problem to be studied further.

ACKNOWLEDGMENT

This work was financially supported by a Grant-in-Aid for Scientific Research (B), (No. 25289285), and a Grant-in-Aid for Scientific Research on Innovative Areas (No. 25105723) from JSPS, and the Program for Element Strategy Initiative for Catalysts & Batteries (ESICB, JPMXP0112101003), commissioned by the MEXT of Japan. S. P. Singh would like to thank JICA for providing the scholarship under FRIENDSHIP project to pursue his Ph.D. in Japan.

REFERENCES

[1] S. Liu, X. Tan, K. Li, R. Hughes, Methane coupling using catalytic membrane reactors, Catal. Rev. - Sci. Eng. 43 (2001) 147–198. doi:10.1081/CR-100104388.

[2] J.J. Spivey, G. Hutchings, Catalytic aromatization of methane, Chem. Soc. Rev. 43 (2014) 792–803. doi:10.1039/c3cs60259a.

[3] X. Guo, G. Fang, G. Li, H. Ma, H. Fan, L. Yu, C. Ma, X. Wu, D. Deng, M. Wei, D. Tan, R. Si, S. Zhang, J. Li, L. Sun, Z. Tang, X. Pan, X. Bao, Direct,Direct,

nonoxidative conversion of methane to ethylene, aromatics, and hydrogen., Science. 344 (2014) 616–9. doi:10.1126/science.1253150.

[4] D. Pakhare, J. Spivey, A review of dry (CO_2) reforming of methane over noble metal catalysts, Chem. Soc. Rev. 43 (2014) 7813–7837. doi:10.1039/c3cs60395d.

[5] S.A.M. Said, M. Waseeuddin, D.S.A. Simakov, A review on solar reforming systems, Renew. Sustain. Energy Rev. 59 (2016) 149–159. doi:10.1016/j.rser.2015.12.072.

[6] T. V. Choudhary, E. Aksoylu, D.W. Goodman, Nonoxidative activation of methane, Catal. Rev. - Sci. Eng. 45 (2003) 151–203. doi:10.1081/CR-120017010.

[7] D. Soulivong, S. Norsic, M. Taoufik, C. Copéret, J. Thivolle-Cazat, S. Chakka, J.M. Basset, Non-oxidative coupling reaction of methane to ethane and hydrogen catalyzed by the silica-supported tantalum hydride: $(\equiv SiO)_2Ta\text{-}H$, J. Am. Chem. Soc. 130 (2008) 5044–5045. doi:10.1021/ja800863x.

[8] K.C. Szeto, S. Norsic, L. Hardou, E. Le Roux, S. Chakka, J. Thivolle-Cazat, A. Baudouin, C. Papaioannou, J.M. Basset, M. Taoufik, Non-oxidative coupling of methane catalysed by supported tungsten hydride onto alumina and silica-alumina in classical and H_2 permeable membrane fixed-bed reactors, Chem. Commun. 46 (2010) 3985–3987. doi:10.1039/c0cc00007h.

[9] L. Yuliati, H. Yoshida, Photocatalytic conversion of methane., Chem. Soc. Rev. 37 (2008) 1592–1602. doi:10.1039/b710575b.

[10] Y. Kato, H. Yoshida, T. Hattori, Photoinduced non-oxidative coupling of methane over silica-alumina and alumina around room temperature, Chem. Commun. (1998) 2389–2390. doi:10.1039/a806825i.

[11] H. Yoshida, Y. Kato, T. Hattori, Photoinduced non-oxidative methane coupling

over silica-alumina, in: Stud. Surf. Sci. Catal., 2000: pp. 659–664. doi:10.1016/S0167-2991(00)81033-2.

[12] H. Yoshida, N. Matsushita, Y. Kato, T. Hattori, Active sites in sol-gel prepared silica-alumina for photoinduced non-oxidative methane coupling, Phys. Chem. Chem. Phys. 4 (2002) 2459–2465. doi:10.1039/b111101a.

[13] Y. Kato, N. Matsushita, H. Yoshida, T. Hattori, Highly active silica-alumina-titania catalyst for photoinduced non-oxidative methane coupling, Catal. Commun. 3 (2002) 99–103. doi:10.1016/S1566-7367(02)00056-0.

[14] H. Yoshida, N. Matsushita, Y. Kato, T. Hattori, Synergistic Active Sites on SiO_2 $-Al_2O_3-TiO_2$ Photocatalysts for Direct Methane Coupling, J. Phys. Chem. B. 107 (2003) 8355–8362. doi:10.1021/jp034458+.

[15] L. Yuliati, T. Hattori, H. Itoh, H. Yoshida, Photocatalytic nonoxidative coupling of methane on gallium oxide and silica-supported gallium oxide, J. Catal. 257 (2008) 396–402. doi:10.1016/j.jcat.2008.05.022.

[16] K. Shimura, H. Yoshida, Semiconductor photocatalysts for non-oxidative coupling, dry reforming and steam reforming of methane, Catal. Surv. from Asia. 18 (2014) 24–33. doi:10.1007/s10563-014-9165-z.

[17] Y. Kato, H. Yoshida, A. Satsuma, T. Hattori, Photoinduced non-oxidative coupling of methane over H-zeolites around room temperature, Microporous Mesoporous Mater. 51 (2002) 223–231. doi:10.1016/S1387-1811(02)00268-8.

[18] H. Yoshida, M.G. Chaskar, Y. Kato, T. Hattori, Active sites on silica-supported zirconium oxide for photoinduced direct methane conversion and photoluminescence, J. Photochem. Photobiol. A Chem. 160 (2003) 47–53. doi:10.1016/S1010-6030(03)00220-X.

[19] L. Yuliati, T. Hamajima, T. Hattori, H. Yoshida, Highly dispersed Ce(III) species on silica and alumina as new photocatalysts for non-oxidative direct methane coupling, Chem. Commun. (2005) 4824–4826. doi:10.1039/b507698f.

[20] L. Yuliati, T. Hattori, H. Yoshida, Highly dispersed magnesium oxide species on silica as photoactive sites for photoinduced direct methane coupling and photoluminescence, Phys. Chem. Chem. Phys. 7 (2005) 195–201. doi:10.1039/b410089a.

[21] L. Yuliati, M. Tsubota, A. Satsuma, H. Itoh, H. Yoshida, Photoactive sites on pure silica materials for nonoxidative direct methane coupling, J. Catal. 238 (2006) 214–220. doi:10.1016/j.jcat.2005.12.002.

[22] L. Yuliati, H. Itoh, H. Yoshida, Modification of Highly Dispersed Cerium Oxides on Silica with Highly Dispersed Titanium Oxides as a New Photocatalyst Design for Nonoxidative Direct Methane Coupling, Chem. Lett. 35 (2006) 932–933. doi:10.1246/cl.2006.932.

[23] L. Yuliati, H. Itoh, H. Yoshida, Photocatalytic direct conversion of methane on silica-titania catalysts, Stud. Surf. Sci. Catal. 172 (2007) 457–460.

[24] L. Yuliati, T. Hamajima, T. Hattori, H. Yoshida, Nonoxidative coupling of methane over supported ceria photocatalysts, J. Phys. Chem. C. 112 (2008) 7223–7232. doi:10.1021/jp712029w.

[25] H. Yoshida, Silica-based quantum photocatalysts for selective reactions, Curr. Opin. Solid State Mater. Sci. 7 (2003) 435–442. doi:10.1016/j.cossms.2004.03.006.

[26] H. Yoshida, Active sites of silica-based quantum photocatalysts for non-oxidative reactions, Catal. Surv. from Asia. 9 (2005) 1–9. doi:10.1007/s10563-005-3330-3.

[27] L. Li, G.D. Li, C. Yan, X.Y. Mu, X.L. Pan, X.X. Zou, K.X. Wang, J.S. Chen,

Efficient sunlight-driven dehydrogenative coupling of methane to ethane over a Zn^{+}-modified zeolite, Angew. Chemie - Int. Ed. 50 (2011) 8299–8303. doi:10.1002/anie.201102320.

[28] S. Wu, X. Tan, J. Lei, H. Chen, L. Wang, J. Zhang, Ga-Doped and Pt-Loaded Porous TiO_2 -SiO_2 for Photocatalytic Nonoxidative Coupling of Methane, J. Am. Chem. Soc. 141 (2019) 6592–6600. doi:10.1021/jacs.8b13858.

[29] L. Meng, Z. Chen, Z. Ma, S. He, Y. Hou, H.H. Li, R. Yuan, X.H. Huang, X. Wang, X. Wang, J. Long, Gold plasmon-induced photocatalytic dehydrogenative coupling of methane to ethane on polar oxide surfaces, Energy Environ. Sci. 11 (2018) 294–298. doi:10.1039/c7ee02951a.

[30] L. Yuliati, H. Itoh, H. Yoshida, Photocatalytic conversion of methane and carbon dioxide over gallium oxide, Chem. Phys. Lett. 452 (2008) 178–182. doi:10.1016/j.cplett.2007.12.051.

[31] T. Yanagida, Y. Sakata, H. Imamura, Photocatalytic Decomposition of H_2O into H_2 and O_2 over Ga_2O_3 Loaded with NiO, Chem. Lett. 33 (2004) 726–727. doi:10.1246/cl.2004.726.

[32] Y. Sakata, Y. Matsuda, T. Nakagawa, R. Yasunaga, H. Imamura, K. Teramura, Remarkable improvement of the photocatalytic activity of Ga_2O_3 towards the overall splitting of H_2O, ChemSusChem. 4 (2011) 181–184. doi:10.1002/cssc.201000258.

[33] Y. Sakata, T. Nakagawa, Y. Nagamatsu, Y. Matsuda, R. Yasunaga, E. Nakao, H. Imamura, Photocatalytic properties of gallium oxides prepared by precipitation methods toward the overall splitting of H_2O, J. Catal. 310 (2014) 45–50. doi:10.1016/j.jcat.2013.06.025.

[34] Y. Hou, X. Wang, L. Wu, Z. Ding, X. Fu, Efficient decomposition of benzene over a β-Ga_2O_3 photocatalyst under ambient conditions, Environ. Sci. Technol. 40 (2006) 5799–5803. doi:10.1021/es061004s.

[35] T. Shao, P. Zhang, L. Jin, Z. Li, Photocatalytic decomposition of perfluorooctanoic acid in pure water and sewage water by nanostructured gallium oxide, Appl. Catal. B Environ. 142–143 (2013) 654–661. doi:10.1016/j.apcatb.2013.05.074.

[36] H. Yoshida, K. Maeda, Preparation of gallium oxide photocatalysts for reduction of carbon dioxide, Stud. Surf. Sci. Catal. 175 (2010) 351–354. doi:10.1016/S0167-2991(10)75058-8.

[37] K. Shimura, T. Yoshida, H. Yoshida, Photocatalytic activation of water and methane over modified gallium oxide for hydrogen production, J. Phys. Chem. C. 114 (2010) 11466–11474. doi:10.1021/jp1012126.

[38] K. Shimura, K. Maeda, H. Yoshida, Thermal Acceleration of Electron Migration in Gallium Oxide Photocatalysts, J. Phys. Chem. C. 115 (2011) 9041–9047. doi:10.1021/jp110824n.

[39] K. Shimura, H. Yoshida, Effect of doped zinc species on the photocatalytic activity of gallium oxide for hydrogen production, Phys. Chem. Chem. Phys. 14 (2012) 2678–2684. doi:10.1039/c2cp23220k.

[40] K. Teramura, H. Tsuneoka, T. Shishido, T. Tanaka, Effect of H_2 gas as a reductant on photoreduction of CO_2 over a Ga_2O_3 photocatalyst, Chem. Phys. Lett. 467 (2008) 191–194. doi:10.1016/j.cplett.2008.10.079.

[41] N. Yamamoto, T. Yoshida, S. Yagi, Z. Like, T. Mizutani, S. Ogawa, H. Nameki, H. Yoshida, The Influence of the Preparing Method of a Ag/Ga_2O_3 Catalyst on its Activity for Photocatalytic Reduction of CO_2 with Water, E-Journal Surf. Sci.

Nanotechnol. 12 (2014) 263–268. doi:10.1380/ejssnt.2014.263.

[42] K. Teramura, Z. Wang, S. Hosokawa, Y. Sakata, T. Tanaka, A doping technique that suppresses undesirable H_2 evolution derived from overall water splitting in the highly selective photocatalytic conversion of CO_2 in and by water, Chem. - A Eur. J. 20 (2014) 9906–9909. doi:10.1002/chem.201402242.

[43] M. Yamamoto, T. Yoshida, N. Yamamoto, T. Nomoto, Y. Yamamoto, S. Yagi, H. Yoshida, Photocatalytic reduction of CO_2 with water promoted by Ag clusters in Ag/Ga_2O_3 photocatalysts, J. Mater. Chem. A. 3 (2015) 16810–16816. doi:10.1039/c5ta04815j.

[44] Y.X. Pan, Z.Q. Sun, H.P. Cong, Y.L. Men, S. Xin, J. Song, S.H. Yu, Photocatalytic CO_2 reduction highly enhanced by oxygen vacancies on Pt-nanoparticle-dispersed gallium oxide, Nano Res. 9 (2016) 1689–1700. doi:10.1007/s12274-016-1063-4.

[45] Z. Wang, K. Teramura, Z. Huang, S. Hosokawa, Y. Sakata, T. Tanaka, Tuning the selectivity toward CO evolution in the photocatalytic conversion of CO_2 with H_2O through the modification of Ag-loaded Ga_2O_3 with a $ZnGa_2O_4$ layer, Catal. Sci. Technol. 6 (2016) 1025–1032. doi:10.1039/c5cy01280e.

[46] Y. Kawaguchi, M. Akatsuka, M. Yamamoto, K. Yoshioka, A. Ozawa, Y. Kato, T. Yoshida, Preparation of gallium oxide photocatalysts and their silver loading effects on the carbon dioxide reduction with water, J. Photochem. Photobiol. A Chem. 358 (2018) 459–464. doi:10.1016/j.jphotochem.2017.11.010.

[47] H. Yoshida, S. Kato, K. Hirao, J.-I. Nishimoto, T. Hattori, Photocatalytic steam reforming of methane over platinum-loaded semiconductors for hydrogen production, Chem. Lett. 36 (2007) 430–431. doi:10.1246/cl.2007.430.

[48] H. Yoshida, K. Hirao, J.-I. Nishimoto, K. Shimura, S. Kato, H. Itoh, T. Hattori,

Hydrogen production from methane and water on platinum loaded titanium oxide photocatalysts, J. Phys. Chem. C. 112 (2008) 5542–5551. doi:10.1021/jp077314u.

[49] K. Shimura, S. Kato, T. Yoshida, H. Itoh, T. Hattori, H. Yoshida, Photocatalytic steam reforming of methane over sodium tantalate, J. Phys. Chem. C. 114 (2010) 3493–3503. doi:10.1021/jp902761x.

[50] A. Yamamoto, S. Mizuba, Y. Saeki, H. Yoshida, Platinum loaded sodium tantalate photocatalysts prepared by a flux method for photocatalytic steam reforming of methane, Appl. Catal. A Gen. 521 (2016) 125–132. doi:10.1016/j.apcata.2015.10.031.

[51] S. Geller, Crystal Structure of β-Ga_2O_3 Cite, J. Chem. Phys. 33 (1960) 676. doi:10.1063/1.1731237.

[52] M. Marezio, J. P. Remeika, Bond lengths in α-Ga_2O_3 structure and high-pressure phase of $Ga_{2-x}Fe_xO_3$, J. Chem. Phys. 46 (1967) 1862. doi:10.1063/1.1840945.

[53] M. Zinkevich, F.M. Morales, H. Nitsche, M. Ahrens, M. Rühle, F. Aldinger, Microstructural and thermodynamic study of γ-Ga_2O_3, Zeitschrift Fuer Met. 95 (2004) 756–762. doi:10.3139/146.018018.

[54] S. Iguchi, Y. Hasegawa, K. Teramura, S. Kidera, S. Kikkawa, S. Hosokawa, H. Asakura, T. Tanaka, Drastic improvement in the photocatalytic activity of Ga_2O_3 modified with Mg-Al layered double hydroxide for the conversion of CO_2 in water, Sustainable Energy Fuels 1 (2017) 1740-1747. doi: 10.1039/c7se00204a.

[55] A. Barrera, F. Tzompantzi, J.M. Padilla, J.E. Casillas, G. Jácome-Acatitla, M.E. Cano, R. Gómez, Reusable PdO/Al_2O_3-Nd_2O_3 photocatalysts in the UV photodegradation of phenol, Appl. Catal. B Environ. 144 (2014) 362–368. doi:10.1016/j.apcatb.2013.07.024.

[56] H. Yoshida, S. Mizuba, A. Yamamoto, Preparation of sodium hexatitanate photocatalysts by a flux method for photocatalytic steam reforming of methane, Catal. Today. 334 (2019) 30–36. doi:10.1016/j.cattod.2019.02.055.

LIST OF TABLE AND FIGURES.

Table 1 Results of photocatalytic reaction test for NOCM over the bare Ga_2O_3 sample and various M(x)/Ga_2O_3 samples.

Fig. 1. XRD patterns of (a) β-Ga_2O_3 from a database (ICSD#34243), (b) the bare Ga_2O_3 sample, and (c-e) the Pd(x)/Ga_2O_3 samples, where x = 0.05, 0.1, and 0.5, respectively.

Fig. 2. SEM images of (A) the bare Ga_2O_3 sample and (B) the Pd(0.5)/Ga_2O_3 sample.

Fig. 3. Diffuse reflectance UV-visible spectra of (a) the bare Ga_2O_3 sample and (b-d) the Pd(x)/Ga_2O_3 samples, where x = 0.05, 0.1, and 0.5, respectively.

Fig. 4. Time courses of the production rate of (a) ethane, r_C, and (b) hydrogen, r_H, and (c) the ratio of these production rates, R=r_C/r_H, in the photocatalytic reaction test for NOCM over the bare Ga_2O_3 sample. Photocatalyst in a quartz cell: 0.8 g. Photoirradiation area: 4 cm^2. Cell volume: 0.4 cm^3. Feed gas: 10% of CH_4 in Ar (total flow rate = 30 mL min^{-1}). Contact time: 0.8 s. Space velocity (SV): 4500 h^{-1}. Light intensity: 20 mW cm^{-2}. The reaction temperature: around room temperature (*ca.* 320 K).

Fig. 5. Time courses of the production rates of (a) ethane and (b) hydrogen, and (c) the ratio of these production rates, *R,* in the photocatalytic reaction test for NOCM over (A) the Pt(0.1)/Ga_2O_3 sample and (B) the Pd(0.5)/Ga_2O_3 sample. The reaction conditions were the same as those described in the caption of Fig. 4.

Fig. 6. Production rates of (a) ethane and (b) hydrogen, and (c) the ratio of these production rates, *R,* in the photocatalytic reaction test for NOCM over the Pd(0.05)/Ga_2O_3 sample at different intensities of incident light. The production

rates were measured after 5 h under photoirradiation in separate reaction tests for photocatalytic NOCM at each intensity of light. The other reaction conditions were the same as those described in the caption of Fig. 4.

Fig. 7. Production rates of (a) ethane and (b) hydrogen, and (c) the ratio of these production rates, *R,* in the photocatalytic reaction test for NOCM over the Pd(0.05)/Ga_2O_3 sample at different concentrations of methane in the feed gas. The production rates were measured after 5 h under photoirradiation in separate reaction tests for photocatalytic NOCM at each concentration of methane. The other reaction conditions were the same as those described in the caption of Fig. 4.

Fig. 8. Production rates of (a) ethane and (b) hydrogen, and (c) the ratio of these production rates, *R,* in the photocatalytic reaction test for NOCM over the Pd(0.05)/Ga_2O_3 sample at different flow rates of the feed gas. The production rates were measured after 5 h under photoirradiation in separate reaction tests for photocatalytic NOCM at each flow rate. The other reaction conditions were the same as those described in the caption of Fig. 4.

Table 1. Results of photocatalytic reaction test for NOCM over the bare Ga_2O_3 sample and various M(x)/Ga_2O_3 samples. [a,b]

Entry	Samples	Production rates [μmol h^{-1}]		R [c]
		C_2H_6	H_2	
1	Ga_2O_3	0.073	0.18	0.41
2	Pt(0.1)/Ga_2O_3	0.023	1.6	0.014
3	Rh(0.1)/Ga_2O_3	n.d. [d]	0.72	
4	Pd(0.05)/Ga_2O_3	0.35	0.85	0.41
5	Pd(0.1)/Ga_2O_3	0.51	1.2	0.42
6	Pd(0.5)/Ga_2O_3	0.22	0.23	0.96
7	Ag(0.1)/Ga_2O_3	0.17	0.23	0.74
8	Ni(0.1)/Ga_2O_3	n.d.[d]	0.10	
9	Fe(0.1)/Ga_2O_3	n.d. [d]	0.13	
10	In(0.1)/Ga_2O_3	0.045	0.20	0.23
11	Zn(0.1)/Ga_2O_3	0.088	0.14	0.63
12	Sm(0.1)/Ga_2O_3	0.049	0.16	0.31
13	Pd(0.5)/Ga_2O_3[e]	n.d.[d]	n.d.[d]	
14	Pd(0.5)/Ga_2O_3[f]	n.d.[d]	n.d.[d]	
15	Pd(0.5)/Ga_2O_3[g]	n.d. [d]	0.36	

[a] Reaction conditions were the same as those described in the caption of Fig. 4. The values of production rates were recorded at 5.5 h later from the start of the photoirradiation. [b] The Ga_2O_3 sample used here was commercially obtained. Various M(x)/Ga_2O_3 samples were prepared by an impregnation method, where x shows loading amount of the additive metal oxide or metals M in wt%, for example, Pd(0.5)/Ga_2O_3. [c] Calculated as follows: R = (production rate of ethane)/(production rate of hydrogen). [d] n.d. = not detected. [e–g] The reaction tests were carried out at 323 K [e], 573 K [f], and 623 K [g], respectively in dark.

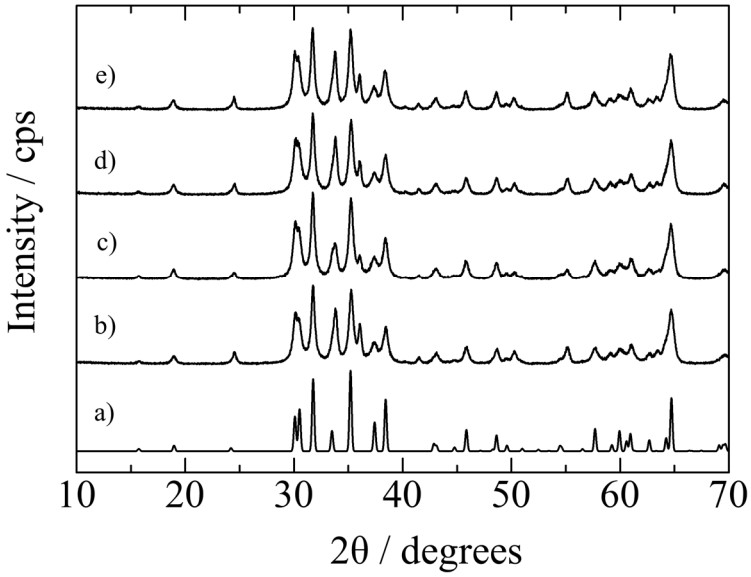

Fig. 1. XRD patterns of (a) β-Ga_2O_3 from a database (ICSD#34243), (b) the bare Ga_2O_3 sample, and (c-e) the Pd(x)/Ga_2O_3 samples; where, x = 0.05, 0.1, and 0.5, respectively.

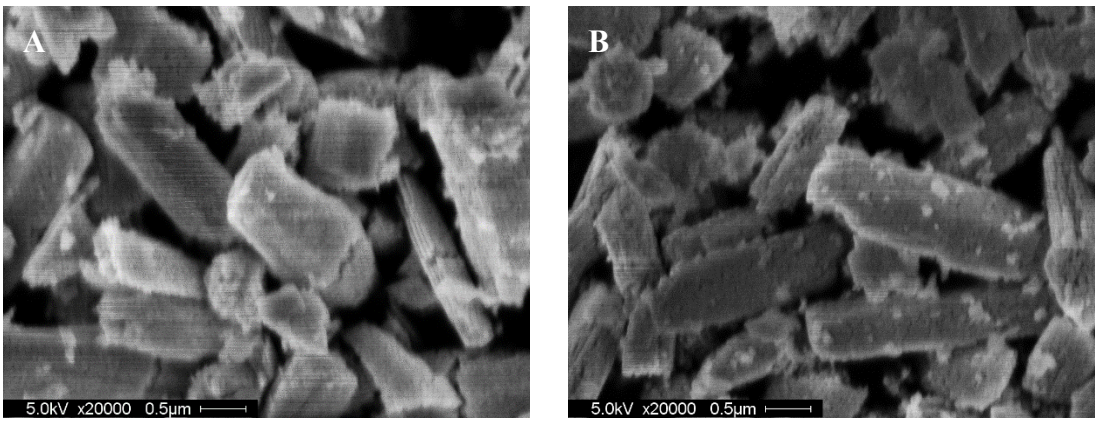

Fig. 2. SEM images of (A) the bare Ga_2O_3 sample and (B) the Pd(0.5)/Ga_2O_3 sample.

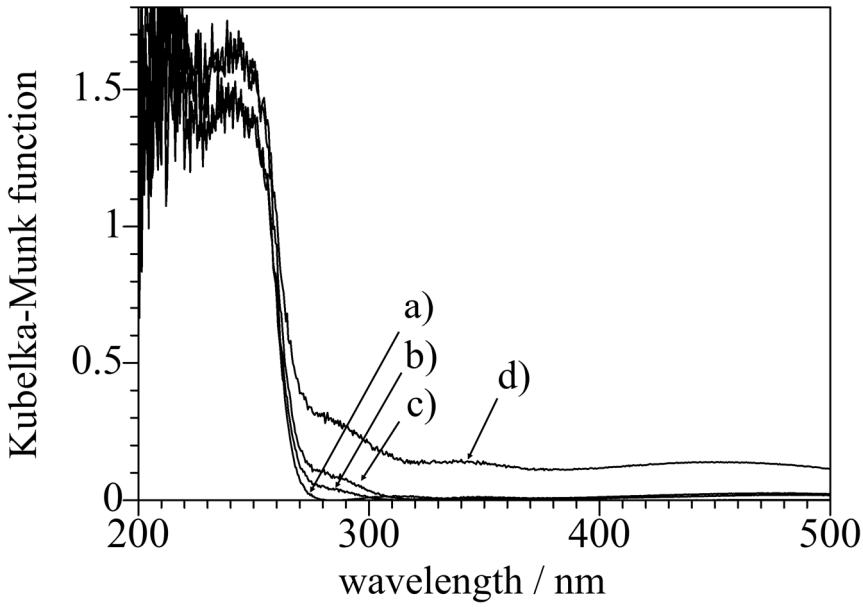

Fig. 3. Diffuse reflectance UV-visible spectra of (a) the bare Ga_2O_3 sample and (b-d) the Pd(x)/Ga_2O_3 samples, where x = 0.05, 0.1, and 0.5, respectively.

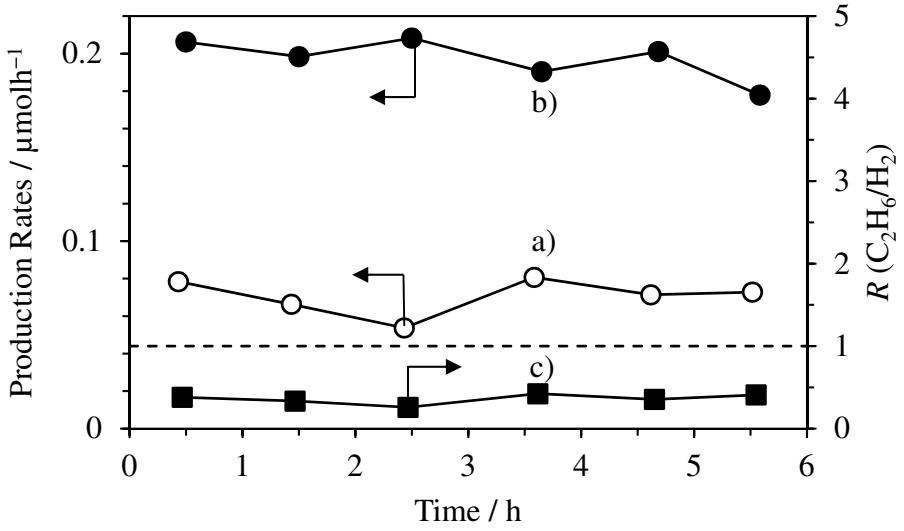

Fig. 4. Time courses of the production rates of (a) ethane, r_C, and (b) hydrogen, r_H, and (c) the ratio of these production rates, R=r_C/r_H, in the photocatalytic reaction test for NOCM over the bare Ga_2O_3 sample. Photocatalyst in a quartz cell: 0.8 g. Photoirradiation area: 4 cm^2. Cell volume: 0.4 cm^3. Feed gas: 10% of CH_4 in Ar (total flow rate = 30 mL min^{-1}). Contact time: 0.8 s. Space velocity (SV): 4500 h^{-1}. Light intensity: 20 mW cm^{-2}. The reaction temperature: around room temperature (*ca.* 320 K).

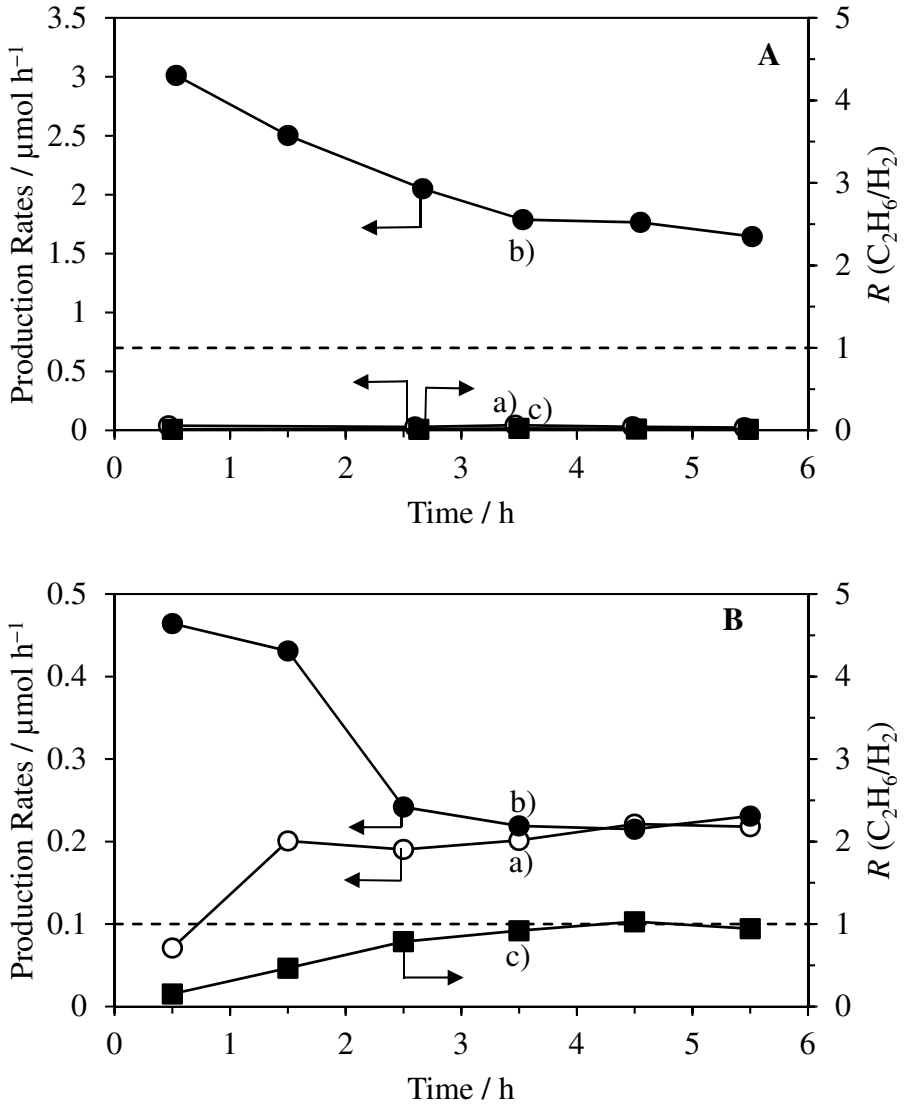

Fig. 5. Time courses of the production rates of (a) ethane and (b) hydrogen, and (c) the ratio of these production rates, *R,* in the photocatalytic reaction test for NOCM over (A) the Pt(0.1)/Ga_2O_3 sample and (B) the Pd(0.5)/Ga_2O_3 sample. The reaction conditions were the same as those described in the caption of Fig. 4.

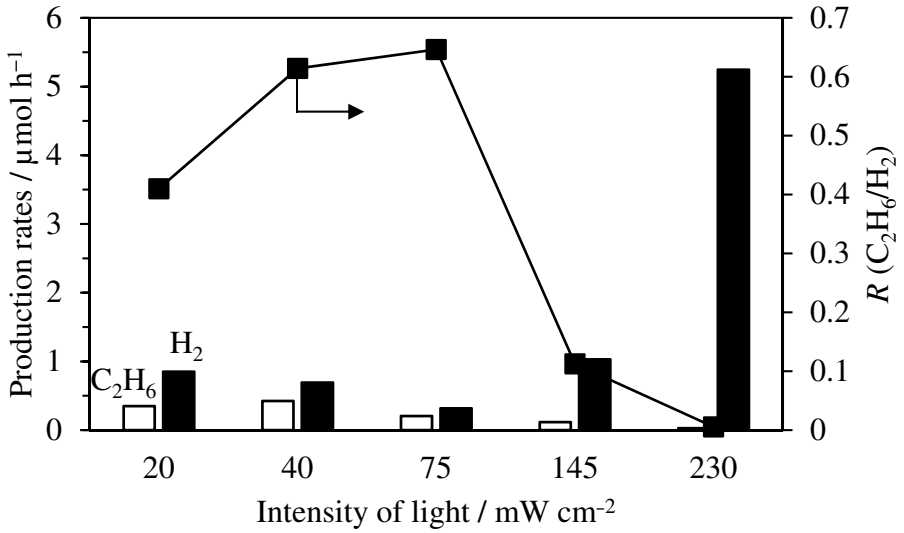

Fig. 6. Production rates of (a) ethane and (b) hydrogen, and (c) the ratio of these production rates, *R,* in the photocatalytic reaction test for NOCM over the Pd(0.05)/Ga_2O_3 sample at different intensities of incident light. The production rates were measured after 5 h under photoirradiation in separate reaction tests for photocatalytic NOCM at each intensity of light. The other reaction conditions were the same as those described in the caption of Fig. 4.

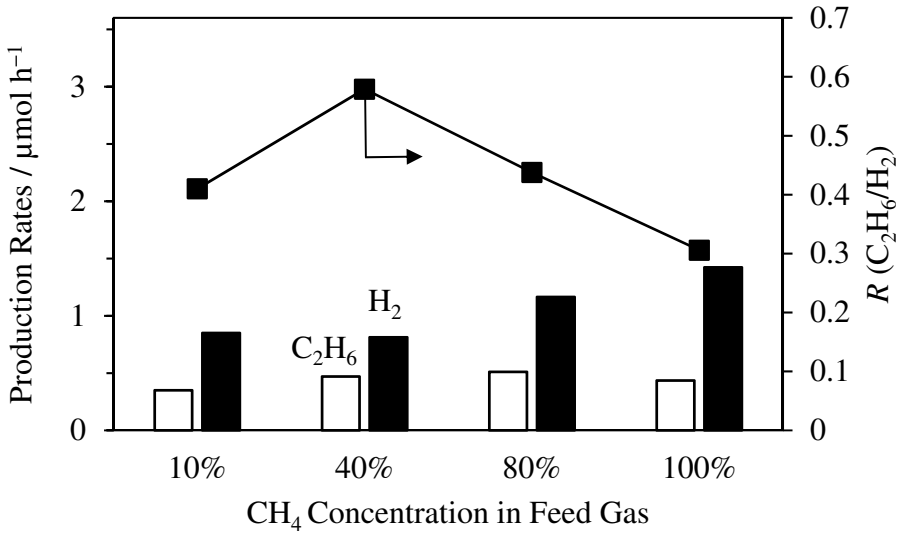

Fig. 7. Production rates of (a) ethane and (b) hydrogen, and (c) the ratio of these production rates, *R,* in the photocatalytic reaction test for NOCM over the Pd(0.05)/Ga_2O_3 sample at different concentrations of methane in the feed gas. The productions rates were measured after 5 h under photoirradiation in separate reaction tests for photocatalytic NOCM at each concentration of methane. The other reaction conditions were the same as those described in the caption of Fig. 4.

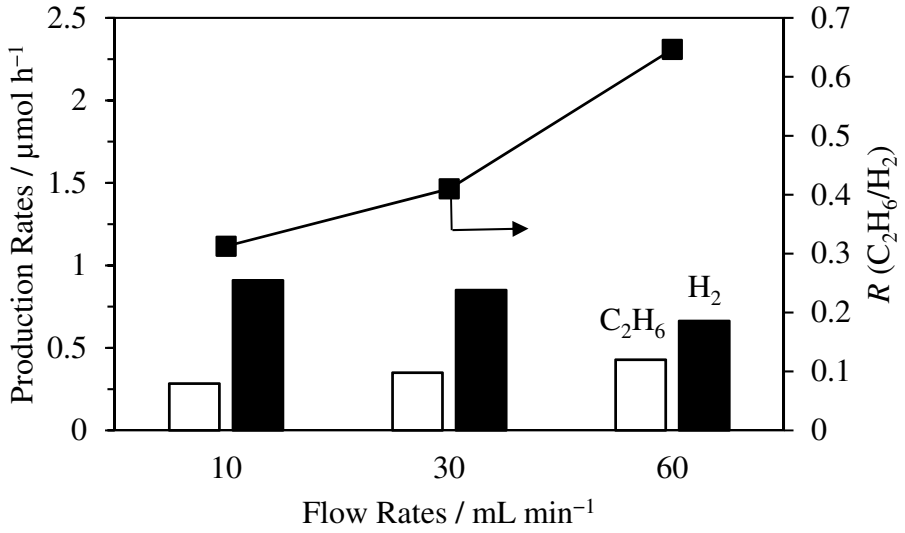

Fig. 8. Production rates of (a) ethane and (b) hydrogen, and (c) the ratio of these production rates, *R,* in the photocatalytic reaction test for NOCM over the Pd(0.05)/Ga_2O_3 sample at different flow rates of the feed gas. The production rates were measured after 5 h under photoirradiation in separate reaction tests for photocatalytic NOCM at each flow rate. The other reaction conditions were the same as those described in the caption of Fig. 4.